Clim Dyn (2011) 36:2147–2158
DOI 10.1007/s00382-010-0926-8

How well do coupled models replicate ocean energetics relevant to ENSO?

Jaclyn N. Brown · Alexey V. Fedorov · Eric Guilyardi

Received: 21 October 2009 / Accepted: 4 October 2010 / Published online: 5 November 2010

Abstract Accurate replication of the processes associated with the energetics of the tropical ocean is necessary if coupled GCMs are to simulate the physics of ENSO correctly, including the transfer of energy from the winds to the ocean thermocline and energy dissipation during the ENSO cycle. Here, we analyze ocean energetics in coupled GCMs in terms of two integral parameters describing net energy loss in the system using the approach recently proposed by Brown and Fedorov (J Clim 23:1563–1580, 2010a) and Fedorov (J Clim 20:1108–1117, 2007). These parameters are (1) the efficiency γ of the conversion of wind power into the buoyancy power that controls the rate of change of the available potential energy (APE) in the ocean and (2) the e-folding rate α that characterizes the damping of APE by turbulent diffusion and other processes. Estimating these two parameters for coupled models reveals potential deficiencies (and large differences) in how state-of-the-art coupled GCMs reproduce the ocean energetics as compared to ocean-only models and data assimilating models. The majority of the coupled models we analyzed show a lower efficiency (values of γ in the range of 10–50% versus 50–60% for ocean-only simulations or reanalysis) and a relatively strong energy damping (values of α^{-1} in the range 0.4–1 years versus 0.9–1.2 years). These differences in the model energetics appear to reflect differences in the simulated thermal structure of the tropical ocean, the structure of ocean equatorial currents, and deficiencies in the way coupled models simulate ENSO.

Keywords ENSO · Energetics · Thermocline · Coupled modeling

J. N. Brown · A. V. Fedorov (✉)
Department of Geology and Geophysics,
Yale University, New Haven, CT, USA
e-mail: Alexey.Fedorov@yale.edu

J. N. Brown
CSIRO Wealth from Oceans National Research Flagship,
Hobart, TAS 7000, Australia

E. Guilyardi
IPSL/LOCEAN (CNRS/IRD/UPMC/MNHN), Paris, France

E. Guilyardi
NCAS, Climate, University of Reading, Reading, UK

1 Introduction

El Niño-Southern Oscillation (ENSO) is the dominant mode of climate variability originating in the tropical Pacific and affecting weather and climate patterns worldwide (e.g. Wang et al. 2004; McPhaden et al. 2006). Our ability to simulate ENSO with coupled general circulation models of the ocean and atmosphere has improved significantly over the last few years. Nevertheless, model simulations of ENSO remain very diverse (e.g. AchutaRao and Sperber 2006; Guilyardi et al. 2009a), which contributes to large uncertainties in our ability to anticipate and explain potential changes in El Niño characteristics. In fact, differences between coupled models are usually larger than the changes projected by each model under global warming conditions (van Oldenborgh et al. 2005; Guilyardi 2006, 2009a; Collins et al. 2010). The reasons for these differences are related to two main factors—our incomplete understanding of ENSO dynamics, and a large number of different tuning parameters and parameterizations in the models that can lead to different physics of simulated El Niño.

Significant efforts are now directed towards defining process-based metrics and diagnostics that can help us understand why ENSO simulations are so different and suggest how we could improve the models (Gleckler et al. 2008; Sun et al. 2008; Lloyd et al. 2009). For instance, several studies use simplified ENSO models driven by coupled GCM outputs to understand the simulated ENSO properties or changes thereof (Philip and van Oldenborgh 2006, 2009; Dewitte et al. 2007; Jin et al. 2006; Kim and Jin 2010). Others use coupled GCM experiments to understand the effect of specific parameterizations on the simulated ENSO (Meehl et al. 2001; Neale et al. 2008; Guilyardi et al. 2009b; Philip et al. 2009).

In the present paper we evaluate two key parameters or diagnostics [originally proposed by Brown and Fedorov (2010a) and Fedorov (2007)] that highlight crucial differences between coupled models in terms of the energetics of the tropical Pacific Ocean. By the ocean energetics we mean the combination of processes associated with the transfer of energy from the winds to the thermocline during La Niña, removal of energy during El Niño, and energy dissipation by various mechanisms.

The budget of potential and kinetic energy for the tropical ocean is given by two simple equations formulated here in terms of anomalies with respect to the climatological state (in such a formulation all variables, including dissipation anomalies, can be both negative or positive):

$$\frac{\partial K}{\partial t} = W - B - D_1 \quad (1)$$

$$\frac{\partial E}{\partial t} = B - D_2 \quad (2)$$

These are not ad hoc identities but exact integral equalities that can be derived from the primitive equations of motion. Detailed explanations of these equations and their derivation are given in Brown and Fedorov (2008, 2010a) and Goddard and Philander (2000).

In this description, anomalous wind power (W) is generated as wind supplies (removes) energy to the ocean by acting in the same (opposite) direction as the surface currents, (see Eq. 1, Fig. 1). A large fraction of anomalous wind power is converted to anomalous buoyancy power (B) associated with vertical mass fluxes that distort isopycnals in the ocean. The rate of change of kinetic energy (K) is negligible (a few percent of available potential energy variations), so that the remaining wind power goes into D_1. For brevity, we will refer to D_1 as turbulent viscous dissipation, which is the main contributor to this term, but D_1 also represents several other types of energy loss including advection of energy out of the tropical basin and loss to the deep ocean. A negative dissipation anomaly means that there is actually less dissipation in the system compared to the mean value.

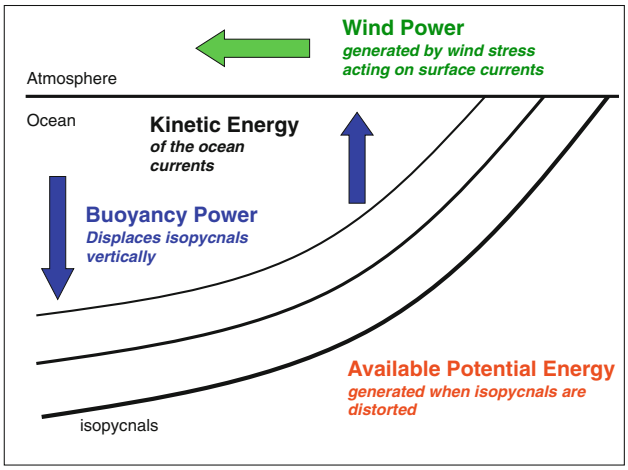

Fig. 1 A general schematic of the ocean energetics. Wind power (i.e. the rate of work, in Watts) is generated by the wind stress acting on surface currents. The wind power modifies the kinetic energy of ocean currents but is mainly converted to buoyancy power (also in Watts). The buoyancy power causes *vertical* displacement of the isopycnals, changing the Available Potential Energy of the ocean (in Joules). This energy estimated for the basin of the tropical Pacific Ocean is largely a measure of the thermocline slope along the equator. After Brown and Fedorov (2010a)

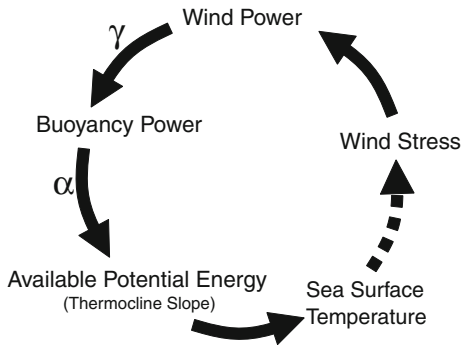

Fig. 2 A schematic of energy cycling in the tropical ocean during ENSO (c.f. Van Oldenborgh et al. 2005). Wind stress induces ocean currents, thus generating wind power anomalies. The wind power anomalies are converted to buoyancy power anomalies with the efficiency γ (in %), see Eqs. (3–5). Variations in buoyancy power modify the available potential energy (subject to damping with the e-folding rate α, in years^{-1}). On ENSO timescales, APE anomalies are related to changes in the thermocline slope along the equator, which induce SST anomalies in the eastern equatorial Pacific (a common index of ENSO). These SST anomalies then drive the wind stress changes as indicated by the *dashed line*—this part of the cycle is described by atmospheric processes and as such is not considered here. After Brown and Fedorov (2010a)

The buoyancy power directly affects the rate of change of Available Potential Energy (E)[1] with a relatively small dissipation anomaly D_2 (Eq. 2). D_2 incorporates turbulent diffusive dissipation and other relevant processes. Thus, the

[1] We use conventional abbreviation APE in the text and notation E in the equations.

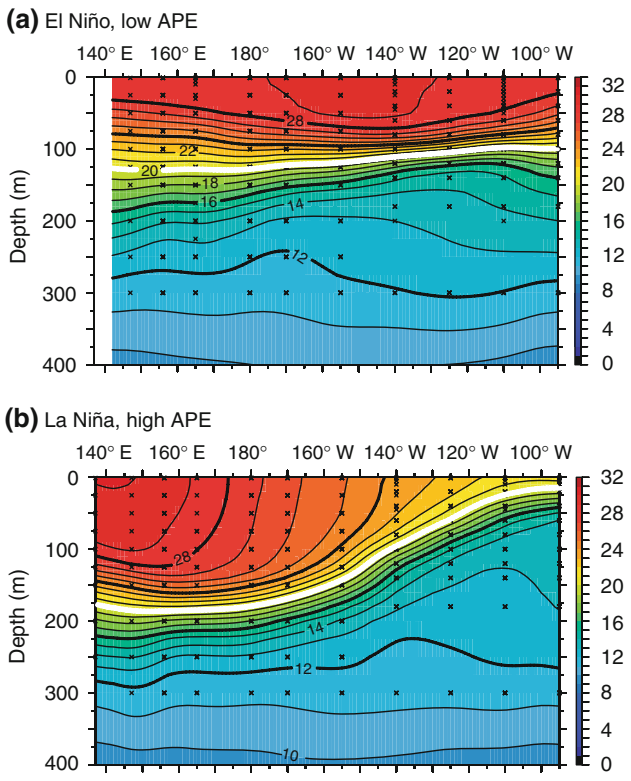

Fig. 3 Ocean thermal structure as a function of depth along the equator at peaks of **a** El Niño, January 1998, corresponding to low available potential energy and **b** La Niña, December 1999, with high available potential energy. The *solid white line* indicates the 20°C isotherm—a good proxy for the thermocline depth along the equator. From the TAO data; see McPhaden (1999) and also Fedorov and Brown (2009)

buoyancy power B acts as a conversion term responsible for converting wind power into the APE (Figs. 1, 2).

It is important to note that in the tropical Pacific, the APE is largely a measure of the thermocline slope along the equator (e.g. Fedorov et al. 2003, Brown and Fedorov 2008). This is one of the reasons why the energetics are useful for studying ENSO as first explored in a important study by Goddard and Philander (2000). A steep thermocline (as during La Niña) implies a positive energy anomaly, and a flat thermocline (El Niño) implies a negative energy anomaly (Figs. 3, 4a). According to Eq. (2) these variations in E are caused by prior anomalies in buoyancy power B induced by wind power anomalies W (positive or negative, respectively).

Brown and Fedorov (2010a) showed that D_1, D_2 and B in Eqs. (1) and (2) can be approximated with a good accuracy as

$$D_1 = (1-\gamma)W, D_2 = \alpha E, \text{and } B = \gamma W; \tag{3}$$

These formulae simply imply that the two dissipation terms, D_1 and D_2, are roughly proportional to wind power and APE, respectively. Note that the first and last expressions in (3) are equivalent as long as the time rate of change of kinetic energy is negligible.

The two parameters, γ and α, describe the integral behavior of the system: γ is the efficiency of the wind power to buoyancy power conversion ($0 < \gamma < 1$) and α is a measure of the damping of APE (α^{-1} gives the e-folding damping timescale in years). Schematically, the energy cycle during ENSO and the roles of γ and α are sketched in Fig. 2. With the use of these two parameters the APE balance in the ocean can be described as

$$\frac{\partial E}{\partial t} = \gamma W - \alpha E \tag{4}$$

Brown and Fedorov (2010a) examined this balance[2] in a range of ocean models, including models forced solely at the ocean surface and models with extensive assimilation of the observed subsurface data. For brevity, we will refer to the former and the latter types as ocean-only models and data assimilations, respectively.

These authors found that the efficiency γ was about 50–60%, whereas α, the damping rate for the APE, was approximately 1 year^{-1}. Differences in the way the models transfer energy were attributed to differences in the imposed wind stress and simulated ocean currents, amongst other model features. The mean depth of the thermocline was noted as another factor, since a shallow thermocline may require only a small energy input to lift cool water to the surface, whereas a deeper thermocline may require larger energy variations.

The goal of this study is to estimate these two parameters for coupled ocean–atmosphere GCMs and explore some differences in the way that the models transfer and dissipate energy on ENSO timescales. We use output from the World Climate Research Programme's (WCRP) Coupled Model Intercomparison Project phase 3 (CMIP3) multi-model dataset, the twentieth century simulations (Meehl et al. 2007). We are interested in whether coupled models behave similarly to forced ocean models, whether there are any consistent features between the models, and what the overall range of energy dissipation characteristics is.

2 Calculations

The three key variables in the energy balance of Eqs. (1) and (2) are wind power W (the rate of work), buoyancy power B, and available potential energy E. As mentioned before, the rate of change of kinetic energy is negligible. Following previous studies (Goddard and Philander 2000;

[2] Fedorov (2007) used a slightly different notation, with 2α as the coefficient in front of E in Eq. (4).

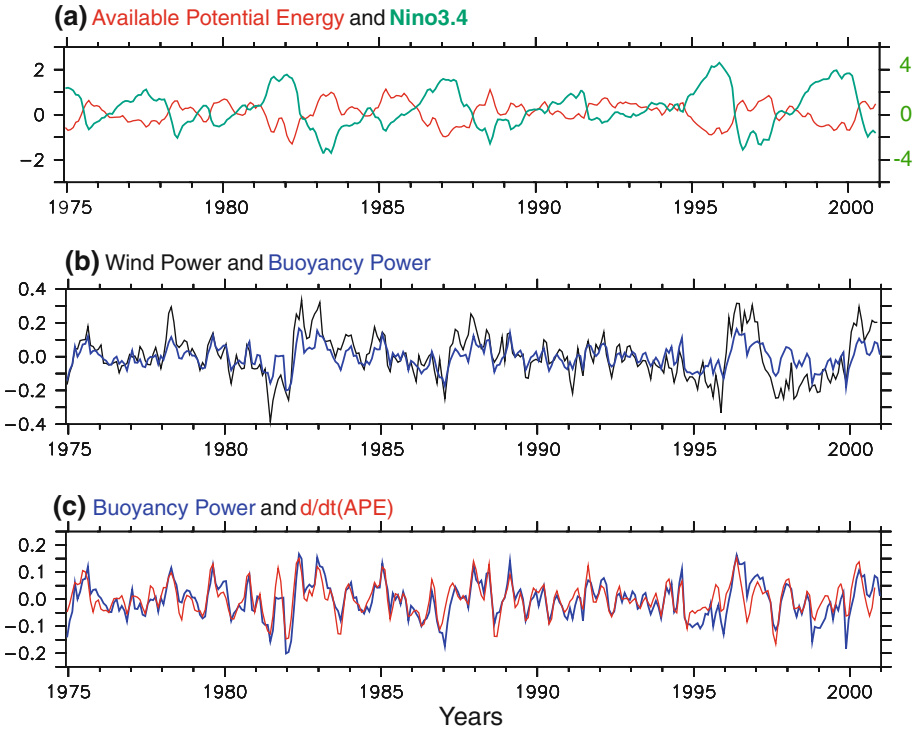

Fig. 4 An example of typical time series showing several variables relevant to the ocean energetics (from a GFDL-CM2.1 twentieth Century run for model years 1975–2000): **a** The available potential energy E and the model's Nino3.4 index (in units of 10^{18} J and °C, respectively). The two are highly anti-correlated, correlation coefficient −0.8. **b** Wind power W and buoyancy power B (in units of Terawatts, 10^{12} W). W and B are highly correlated but the signal is attenuated when going from W to B (note the difference between the *black* and the *blue lines*). The attenuation is described by the efficiency γ. **c** Buoyancy power B and the rate of change of APE (dE/dt, in Terawatts). The difference between dE/dt and B is the energy loss D_2 (i.e. the difference between the *red* and the *blue lines*)

Fedorov et al. 2003; Fedorov 2007; Brown and Fedorov 2008, 2010a) we calculate these variables as follows.

The wind power (in Watts) in Eq. (1) is defined as the dot product of the wind stress, $\boldsymbol{\tau} = (\tau^x,\tau^y)$, and the surface current $\mathbf{u} = (u,v)$, integrated over the surface A of the tropical Pacific basin:

$$W = \iint \mathbf{u}\boldsymbol{\tau}\, dA \tag{5}$$

Typically, we neglect the meridional contribution to (5). Note that previous studies (Dawe and Thompson 2006; Zhai and Greatbatch 2007) have suggested that including ocean surface currents in the bulk formula for the wind stress can be important for calculating wind power. Some models we considered do take ocean currents into account (e.g. GFDL-CM2.1), some do not. However, for the parameters γ and α, we anticipate this effect to be minor since these parameters depend on on processes involved in energy conversion rather than on the absolute values of W.

A significant proportion of the wind power is converted to buoyancy power (in Watts), defined as

$$B = \iiint (\rho - \rho^*) g w\, dV \tag{6}$$

where the integral is taken over the volume V of the tropical Pacific basin in the upper ocean that extends to 400 m depth. Here, w is the vertical velocity, g is gravity, and ρ is potential density. The horizontal average, $\rho^*(z)$, is the reference potential density obtained by averaging ρ over x, y and t in the basin of interest.

The available potential energy, E, is defined in terms of potential density in accordance with Oort et al. (1989) as

$$E = \iiint \frac{1}{2} \frac{(\rho - \rho^*)^2}{S^2} dV, \tag{7}$$

where the stability factor, $S^2 = -\frac{1}{g}\frac{d\rho^*}{dz}$, is proportional to the buoyancy frequency. We use potential rather than in situ density in these calculations, which may make a difference when estimating the vertical density gradient in (7). After calculating E, W and B we subtract the annual cycle of these variables in order to obtain interannual anomalies.

The horizontal boundaries of the tropical basin are defined as 140°E to the coast of South America and from 15°S to 15°N. While other choices of boundaries are possible, Brown and Fedorov (2010a) show that this is an optimal configuration capturing the major contributing factors for W and E and at the same time avoiding the

Table 1 Details of the ocean-only models, data assimilating ocean models and coupled models, including the ocean resolution (longitude, latitude) and, if different, the model resolution near the equator

Model/data product	Originating group(s)	Ocean resolution	Wind stress	Reference
Ocean models				
NEMO/ORCA05a	LOCEAN, IPSL, France	0.5° × 0.5°	NCEP/NCAR	Barnier et al. (2006)
NEMO/ ORCA05b,	LOCEAN, IPSL, France	0.5° × 0.5°	ERA40	Barnier et al. (2006)
MOM4	GFDL, NOAA, US	1° × 1/3°	NCEP/NCAR	Griffies et al. (2005)
POP	LANL/NCAR, US	1.125° × 1/4°	NCEP/NCAR + satellite products	Collins et al. (2006)
Data assimilations				
ECCO	MIT/JPL, US	1° × 1°	NCEP/NCAR	Wunsch and Heimbach (2007)
GODAS	CPC, NOAA, US	1° × 1/3°	NCEP/NCAR	Behringer (2007)
Coupled models				
CCCMA3.1 (T63)	CCCMA, Canada	1.85° × 1.85° L29		Kim et al. (2002)
CCSM3	NCAR, US	1.1° × 1.1° (0.27°) L40		Collins et al. (2006)
CNRM-CM3	CNRM, France	2° × 2° (0.5°) L31		Salas-Mélia (2002)
CSIRO-Mk3.5	CSIRO, Australia	1.9° × 0.8° L31		Gordon et al. (2002)
GFDL-CM2.1	GFDL, NOAA, US	1° × 1° (0.33°) L40		Delworth et al. (2006)
GISS-ER	GISS, NASA, US	4° × 5° L20		Schmidt et al. (2006)
UKMO-HadGem1	Hadley Centre, UKMO, UK	1° × 1° (0.33°) L40		Johns et al. (2004)
INGV-SXG	INGV, Italy	2° × 2° (0.5°) L31		Gualdi et al. (2008)
IPSL-CM4	LOCEAN, IPSL, France	2° × 2° (0.5°) L31		Marti et al. (2005)
MIROC3.2(med)	CCSR/NIES/FRCGC, Japan	1.4° × 0.5° L43		Hasumi and Emori (2004)

Where relevant, the wind stress product used to force a particular model is also shown. Note that many research groups often modify the original wind stress data before applying it as a forcing for their models. NEMO/ORCA05a,b are referred to in the text as ORCAa and b

direct effect of the western boundary current in the West (which would increase the level of noise in the system).

The efficiency γ can be estimated as the least-squares fit between the time series of the buoyancy power B and wind power W:

$$\gamma = \frac{\langle BW \rangle}{\langle W^2 \rangle} \tag{8}$$

The damping coefficient α is estimated via the least-squares fit between E and the dissipation term D_2:

$$\alpha = \frac{\langle ED_2 \rangle}{\langle E^2 \rangle} \tag{9}$$

The brackets in (8) and (9) denote a time average.

These parameters are computed offline using monthly data available from the CMIP3 project. Even though some of the information might be lost when using this resolution compared to weekly data for example, the same temporal resolution in all calculations allows a consistent treatment of different models (we are planning to revisit the issue of data resolution elsewhere). Before further calculations, a 5-point triangular filter is applied to the time series of W, B and E (to eliminate high-frequency noise) and then these time series are de-trended.

Further, the models we compare have different spatial resolutions, but we did not find any obvious link between the spatial resolution and energy balance. Yet, in principle, how well the ocean equatorial currents are resolved can become important for estimating the wind power and buoyancy power. Details and the full names of the analyzed models are provided in Tables 1 and 2.

3 Results

3.1 Interannual variability of W, B and E

The objective of this paper is to examine ocean energetics in coupled models on timescales relevant to ENSO. To that end, let us first look at the interannual variability of the key energy variables. As expected, all models exhibit a robust interannual signal in W, B and E, albeit a bit noisier for the first two variables (e.g. Fig. 4).

Table 2 Summary of the main energy diagnostics for each model. Before computing these values, we subtract the seasonal cycle from the original time series and then apply a five-point triangular filter to eliminate high-frequency noise

Models	Correlation *Nino3.4 SST* and E	Efficiency γ (%)	Correlation B and W	Damping timescale α^{-1} (years)	Correlation D_2 and E
Ocean models					
NEMO/ORCA05a	−0.83	54	0.95	0.9	0.70
NEMO/ORCA05b	−0.81	59	0.94	1.0	0.59
MOM4	−0.74	57	0.91	1.0	0.68
POP	−0.81	33	0.91	1.2	0.59
Data assimilating models					
ECCO	−0.55	56	0.91	1.2	0.56
GODAS	−0.76	50	0.93	–	–
Coupled models—twentieth century					
CCCMA3.1 (T63)	−0.73	36	0.62	0.85	0.67
CCSM3	−0.86	48	0.85	0.92	0.49
CNRM-CM3	−0.91	53	0.84	0.57	0.84
CSIRO-Mk3.5	−0.85	45	0.71	0.57	0.76
GISS-ER	−0.17	14	0.57	–	–
GFDL-CM2.1	−0.80	36	0.77	0.79	0.69
HadGEM1	−0.69	33	0.68	0.89	0.54
INGV-SXG	−0.91	48	0.95	0.48	0.91
IPSL-CM4,	−0.90	44	0.80	0.41	0.86
MIROC3.2(med)	−0.75	37	0.82	1.0	0.52

Note that GODAS (a data assimilating ocean model) produces a negative value of α, which is unphysical, whereas GISS-ER (a coupled model) produces a correlation between D_2 and E that is not statistically significant. As such, these two results are excluded from consideration. Also note the low correlation between *Nino3.4 SST* and E for GISS-ER

The magnitude of interannual variability in both wind and buoyancy power varies greatly between the models, as reflected in the extent of the scatter in monthly data on the B–W plane (Fig. 5). For example, for wind power, GFDL-CM2.1 shows variations of the order of ±0.4 TW, while GISS-ER and Miroc3.2(med) exhibit much weaker variations of the order of ±0.1 TW. Likewise, the amplitude of APE fluctuations can differ by a factor of 4 or 5 between the models (Fig. 7). Often, stronger variations in W translate into stronger variations in E, but such a connection does not hold for every model because each has different efficiency and energy damping rate.

Similar differences were found between the ocean-only models, which depended to a large degree on whether the NCEP wind stress (or its modification) was applied (MOM4, POP, and ORCAa) or the ERA-40 (ORCAb), see Brown and Fedorov (2010a). However, regardless of the forcing input, the overall simulation of ENSO events as seen, for example, in Nino3.4 SST index was not too dissimilar in different ocean-only models and data assimilations. This is obviously not the case for coupled models, which show a considerable diversity of ENSO-like behavior (e.g. Guilyardi et al. 2009a).

3.2 Conversion of wind power to buoyancy power

In each ocean or coupled model, a large fraction of wind power W is converted directly to buoyancy power B (Fig. 4b), which can be described by the efficiency γ of the wind power to buoyancy power conversion. This parameter can be measured as a least-squares fit between B and W (Fig. 5). Ocean-only models and data assimilations have efficiency around 50–60%, with the correlation between wind and buoyancy power higher than 0.9 (Fig. 6; Table 2). The only exception is the POP model with $\gamma \approx 33\%$, probably because of the equatorial thermocline depth being too shallow and close to the mixed layer depth (as discussed later).

The efficiency of the W–B conversion in coupled models varies widely, but tends to be significantly lower (in the range of 10–50%) than the efficiency of the ocean-only models and data assimilations (Fig. 6; Table 2). In most of the coupled models, the correlation between the wind power and buoyancy power is also much lower, which goes together with the reduced efficiency.

3.3 APE damping

Once a buoyancy power anomaly is generated it works to alter the rate of change of APE in the system (Fig. 4c, Eq. 2). On interannual timescales the changes in E are closely reflected by the Nino3.4 index (Fig. 4a). A small proportion of buoyancy power, D_2, is lost in the conversion from B to dE/dt. This energy dissipation, D_2, has been found in ocean models to be almost linearly related to the

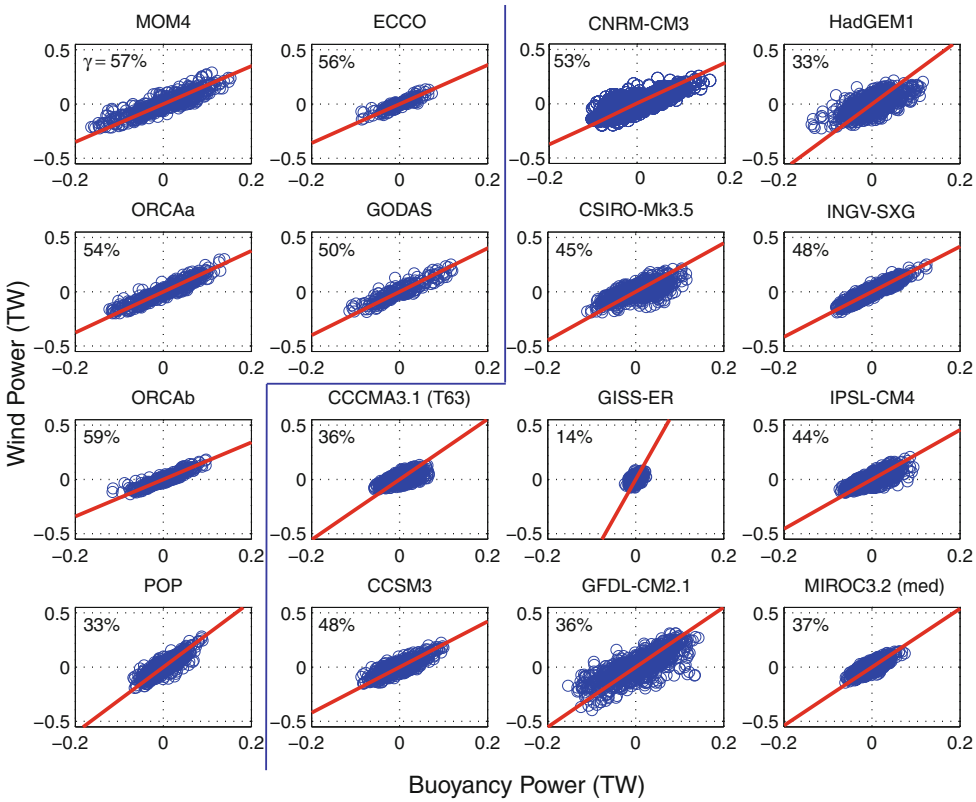

Fig. 5 Estimation of the efficiency γ of wind power to buoyancy power conversion for different models. *Panels* with data from coupled models are to the *right* of the *vertical line*. After the seasonal cycle was subtracted, a five-point *triangular* filter is applied to the original time series to eliminate high-frequency noise. The efficiency γ, labeled at the *upper-left* corner of each plot, is found using the least-squares method (efficiency is estimated as the inverse of the slope of the *red lines*). In a simple linear model $B \approx \gamma W$

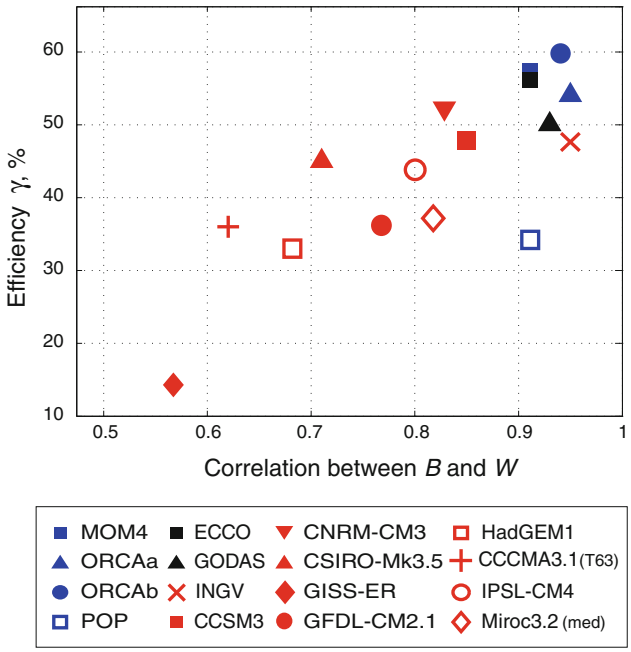

Fig. 6 The efficiency, γ, of the wind power to buoyancy power conversion plotted as a function of the correlation between wind power and buoyancy power for each model. The efficiency indicates how much energy is transferred from the winds to the ocean thermocline in the tropical Pacific on ENSO timescales. Coupled models (in *red*) tend to be less efficient and have a lower correlation between B and W than ocean models with or without data assimilation (*blue* and *black*, respectively). Exact values and the full names of the analyzed models are provided in Tables 1 and 2

anomaly in E, that is $D_2 \approx \alpha E$ (Fig. 7) where α is the APE damping rate. Note that in the context of the ocean shallow-water equations, $\alpha/2$ can be interpreted as a damping rate for thermocline depth anomalies (Fedorov 2007).

Ocean-only models have the APE damping timescale, α^{-1}, of around 1 year, whereas coupled models vary widely in their values for α^{-1} (Fig. 8; Table 2). Many coupled models have a much shorter damping timescale, meaning that thermocline anomalies are damped more quickly. Models such as IPSL-CM4 or INGV-SXG display a very tight connection between E and D_2 with a strong damping of thermocline anomalies. Other models such as GISS-ER show very little connection between APE variations and energy loss. Note that nominally negative values of α would imply that either the regression fails (too low correlation between E and D_2), or there exist artificial sources of energy as likely in the case of data assimilation of GODAS. This latter example underlines how assimilating subsurface ocean data can potentially modify ocean physics.

3.4 Energy balance and the mean thermocline depth

As mentioned already, in the equatorial Pacific the APE variability is a measure of changes in the east–west thermocline slope. During La Niña the thermocline becomes steeper and the APE higher and conversely during El Niño.

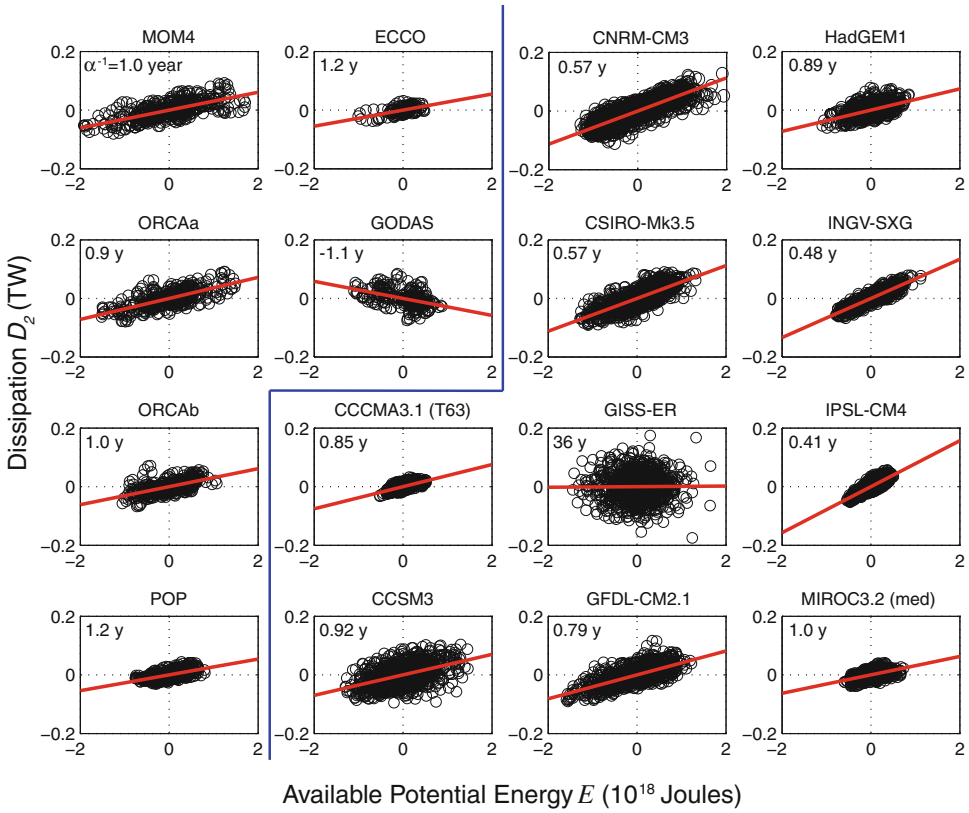

Fig. 7 Estimation of the APE damping timescale α^{-1} for different models (labeled at the *upper-left* corner of each plot). *Panels* with data from coupled models are to the *right* of the *vertical line*. After the seasonal cycle was subtracted, a five-point *triangular* filter is applied to the original time series to eliminate high-frequency noise. The damping rate α (in year^{-1}) is calculated as the slope of the lines obtained as the least-squares fit between D_2 and E. The energy loss D_2 is estimated as the difference between the rate of change of E and buoyancy power B, that is, $-D_2 = dE/dt - B$. In a simple linear model $D_2 \approx \alpha E$. Note that GODAS produces a negative value of α, which is unphysical, whereas GISS-ER shows a correlation that is not statistically significant (the scatter of data points is too broad)

Typically, models that display greater variance in E have larger oscillations of the thermocline slope. In fact, ocean models and almost all coupled models exhibit a very high correlation between the APE and the Nino3.4 SST, with the correlation coefficient in the range -0.7 to -0.9 (Fig. 4a; Table 2). Consequently, the APE provides a reliable proxy for the simulated ENSO.

Not all models have the same mean thermocline depth (Fig. 9). Brown and Fedorov (2010a) found that ocean models that have a deeper thermocline require larger APE variability to generate the same ENSO anomaly. That is, to bring a cold anomaly to the surface, a model with a deep thermocline may require a larger change in the APE.

Our present analysis (that now includes coupled models) shows results reasonably consistent with the above conclusions. Generally, models with a shallower mean thermocline (such as IPSL-CM4 and CCCMA3.1-T63), display only weak variability in E (Fig. 10). The CCSM3 and GFDL-CM2.1 models, on the other hand, have a stronger E signal and a deeper thermocline. Note that the differences between the models in the way they simulate the mean thermocline depth are quite large—from 50 m to some 130 m. Here, we estimate the mean thermocline depth as the location of the maximum of $d\rho^*/dz$ with ρ^* averaged over the tropical basin (between 15°S and 15°N), see Fig. 9. In principle, some of the differences in the simulated thermocline depths can be explained by different vertical mixing in the tropical ocean (e.g. Brierley et al. 2009; Fedorov et al. 2010) or extra-tropical effects that can alter the thermocline depth by modifying the ocean heat budget (Boccaletti et al. 2004) and meridional density gradient (Fedorov et al. 2004; Fedorov 2007).

4 Discussion and conclusions

For a range of coupled ocean–atmosphere GCMs, we have estimated two key parameters that reflect ocean energetics relevant to ENSO—the efficiency γ of energy transfer from winds to the thermocline and the damping rate α for APE anomalies (Figs. 6, 8; Table 2). These parameters constitute the energy-based diagnostics that emphasize differences in the way models represent the cycling of mechanical energy during ENSO. These metrics provide basin-wide physical, integrated measures of the energy loss at different stages of energy transfer from the winds to the thermocline.

In each model the energy balance is unique but can be consistently traced through the system (Fig. 2): The winds remove or supply energy to the thermocline, changing its slope along the equator. Turbulent dissipation (viscous and diffusive) and advection out of the control volume modify the energy transfer, changing the fraction of energy converted to buoyancy power and then to the APE (Table 2),

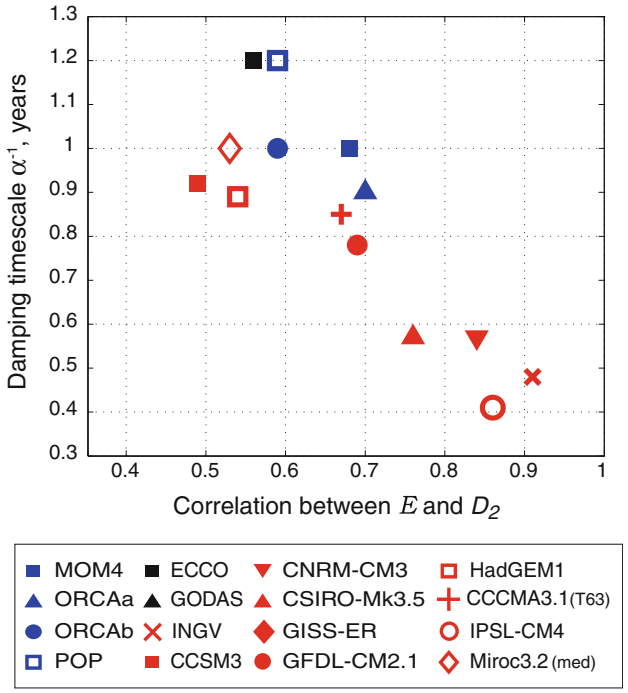

Fig. 8 The damping timescale α^{-1} (in years) plotted as a function of the correlation coefficient between E and diffusive dissipation D_2. Stronger correlation typically corresponds to shorter damping timescales (or stronger damping rates). Coupled models (in *red*) tend to have greater damping than ocean models with or without data assimilation (*blue* and *black*, respectively). Exact values and the full names of the analyzed models are provided in Table 2. Note that GODAS (a data assimilation) produces a negative value of α, which is unphysical, whereas GISS-ER (a coupled model) shows a correlation that is not statistically significant. As such, these two results are excluded from the *graph*

which affects temperatures in the eastern equatorial Pacific (e.g. the Nino3.4 index).

We find that coupled models are less efficient (small γ) than forced ocean models (with or without data assimilation) at converting wind power to buoyancy power. We find values of γ in the range of 10–50% for coupled models versus 50–60% for ocean-only simulations. In some coupled models the percentage of energy generated by wind work at the surface that reaches the thermocline is 2–3 times smaller than the corresponding percentages for forced ocean models.

For many coupled models small efficiency is related to a lower correlation between the wind and buoyancy powers. The reduced correlation can indicate that either coupled models have too much noise uncorrelated with thermocline motion or perhaps that the thermocline (or remote) mode critical for ENSO dynamics is relatively weak in comparison with the SST (or local) mode (e.g. Fedorov and Philander 2001; Guilyardi 2006; also Fedorov 2010).

A majority of coupled models have greater damping of the APE (large α) than ocean-only models and data assimilations. The damping timescale for the APE suggested by ocean models is 1 year, whereas a number of coupled models give the damping timescale of the order of 0.5 years or smaller. Note that this is a nominal damping timescale caused by diffusive dissipation and several other processes. The actual decay or growth rate of E in a decaying or growing oscillation will be determined by a combination of both negative and positive feedbacks of ocean–atmosphere interactions (e.g. Fedorov and Philander 2000, 2001; Thompson and Battisti 2000, 2001; Jin et al. 2006; Philip and van Oldenborgh 2006; Sun et al. 2008; Lloyd et al. 2009; and Fedorov 2010).

Tentative clues for the differences between the model energetics are provided by differences in the simulated ocean thermal structure, and the mean depth of the thermocline in particular (Figs. 9, 10). Large oscillations in the APE that can occur in models such as CCSM3 and GFDL-CM2.1 are possible with a deep mean thermocline. Models with a shallow mean thermocline, such as IPSL-CM4 and CCCMA3.1(T63), have weaker variations in the APE.

Differences in mean thermocline depth obviously do not give a full explanation for our findings since the ocean-only models also have somewhat different thermocline depths. In the present study we also see very different vertical structure of the equatorial currents U(z) at the equator and mean ocean stratification ρ(z) (Fig. 9). These two fields, one more local and the other more global, should affect the strength of vertical and horizontal turbulent mixing of heat and momentum, which depends on the bulk Richardson numbers and hence the vertical gradients of U and ρ (e.g. Large et al. 1994). In addition, ρ(z) should affect the APE calculations. In fact, reproducing both U(z) and ρ(z) very accurately as compared to the observation is a difficult task even for ocean-only models (e.g. Brown and Fedorov 2010b).

Similarly, the study of Brown and Fedorov (2008) showed that the horizontal structure of the ocean currents produced by coupled models could be also quite different from that given by the observations/forced ocean models. However, these relationships between ocean stratification and vertical shear and ocean vertical mixing are not straightforward and highly nonlinear—a further study is necessary to explore these in detail. It is important that although the problem we are considering is of oceanic nature, in a coupled system both U and ρ will are influenced by the winds and therefore the effects of the ocean and the atmosphere become difficult to separate.

The coupled models analyzed here exhibit a large diversity of simulated variance of the Nino3 SST anomaly, as compared to the observations (van Oldenborgh et al. 2005; Guilyardi et al. 2009a). This diversity has several origins. Atmospheric feedbacks where shown to play a role in the simulated ENSO amplitude (e.g. Sun et al. 2008; Lloyd et al. 2009; Guilyardi et al. 2009b) and can

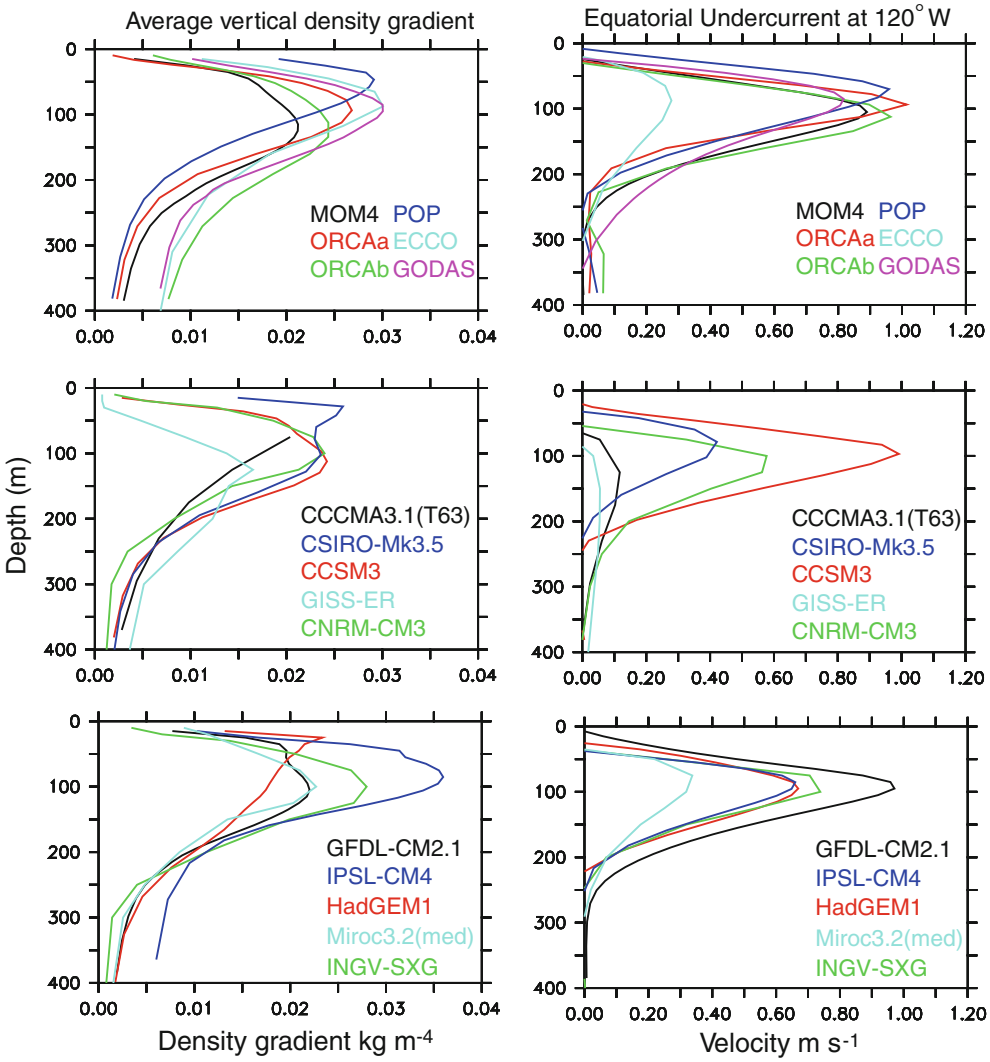

Fig. 9 *Left panels* vertical density gradient as a function of depth for each model. The maximum of dρ*/dz in each case gives the depth of the ocean tropical thermocline (or more accurately pycnocline). The density, ρ*, is an average over 140°E to 70°W and between 15°S and 15°N. *Right panels* the profile of the mean zonal velocity u(z) showing the Equatorial Undercurrent at 120°W. Note that in HadGEM1 the mixed layer and thermocline depth are not clearly defined and so the depth of an approximate isopycnal was chosen to represent the thermocline in later analysis. The weak current in ECCO is related to the model's coarse resolution near the equator

contribute to this diversity. Other studies explored the role of both oceanic and atmospheric processes using simplified ENSO frameworks (Philip and van Oldenborgh 2006; Philip et al. 2009; Kim and Jin 2010; Roberts and Battisti 2010). The analysis of energetics presented here complements those studies and further suggests how the ocean-integrated feedbacks can contribute to this diversity.

A fundamental question that remains open is what the real-world values of the parameters γ and α are. It is unlikely that we will have observations of the ocean thermal structure, winds and surface currents in the tropics with sufficient quality and duration that would allow direct calculations of these parameters any time soon. Energy-conserving data-assimilating ocean model (such as ECCO) could provide perhaps the closest values to those one could expect for the real ocean (and this is the view the present paper takes). However, one might argue that substantial errors in the surface forcing used by those models (wind stress, heat fluxes) and a lack of proper physics (active ocean–atmosphere interactions) would reduce the accuracy of the results obtained by data-assimilating models.

The range of variations of γ and α between coupled models is obviously quite large. This broad range can be both due to biases in the wind field generated by atmospheric GCMs and different parameterizations (of turbulent diffusion and friction) in ocean GCM. Model developers should try to narrow this range and explore how changes in model parameters or resolution will change these

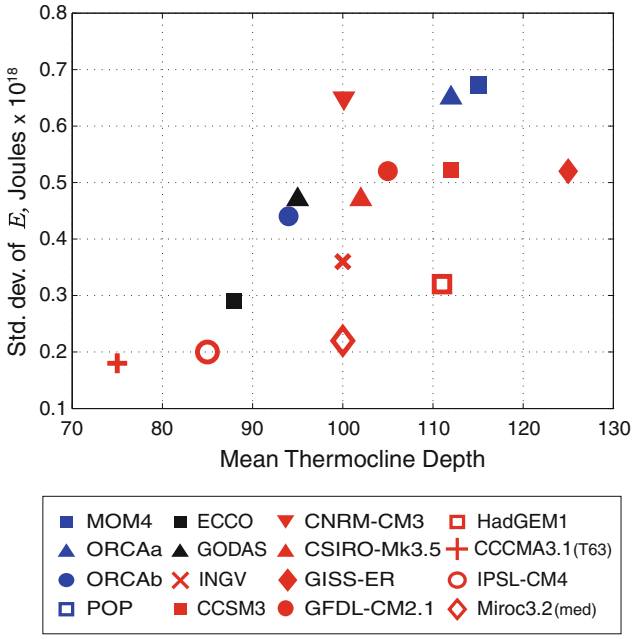

Fig. 10 Standard deviation of available potential energy E as a function of the mean thermocline depth for each model. Thermocline depth is estimated as the depth of the maximum $d\rho^*/dz$. Models with a deeper thermocline tend to have larger variability in E. The POP model is not shown, having too shallow pycnocline

characteristics. Accordingly, we propose that climate modelers regularly calculate these two energy-based parameters and report them among the key metrics, diagnostics and "benchmarks" of the coupled GCMs.

Acknowledgments We acknowledge the modeling groups, the Program for Climate Model Diagnosis and Intercomparison (PCMDI) and the WCRP's Working Group on Coupled Modelling (WGCM) for their roles in making available the WCRP CMIP3 multi-model dataset. Support of this dataset is provided by the Office of Science, US Department of Energy. We would like to thank Mat Maltrud for his tireless assistance setting up and running the POP model at Yale University. In addition, we thank Brian Dobbins for his help running and processing model data. We also thank Gurvan Madec for supply the ORCA data and advice, John Dunne for the MOM4 ocean model output, and George Philander, Lisa Goddard and Remi Tailleux for discussions of this topic. We are grateful to Mat Collins and anonymous reviewers for carefully reviewing the paper. ECMWF ERA-40 data used in this study have been obtained from the ECMWF data server, http://data.ecmwf.int/data/d/era40_mnth. The ECCO data assimilation was provided by the Consortium for Estimating the Circulation and Climate of the Ocean funded by the National Oceanographic Partnership Program (NOPP). We also thank NCAR for providing the NCEP Global Ocean Data Assimilation (GODAS) product. This research was supported in part by grants to AVF from NSF (OCE-0901921), Department of Energy Office of Science (DE-FG02-06ER64238, DE-FG02-08ER64590), the David and Lucile Packard Foundation, and CNRS (France) and by grants to EG from the European Community ENSEMBLES (GOCE-CT-2003-505539) under the Sixth Framework Programme and by the CNRS PICS CORDIAL project.

References

AchutaRao K, Sperber KR (2006) ENSO simulation in coupled ocean-atmosphere models: are the current models better? Clim Dyn 27:1–15

Barnier B, Madec G, Penduff J-MM, Treguier AM, Le Sommer J, Beckmann A, Biastoch A, Boning C, Dengg J, Derval C, Durand E, Gulev S, Remy E, Talandier C, Theetten S, Maltrud M, McClean JL, De Cuevas B (2006) Impact of partial steps and momentum advection schemes in a global ocean circulation model at eddy-permitting resolution. Ocean Dyn 56(5–6):543–567

Behringer DW (2007) The global ocean data assimilation system at NCEP, 11th symposium on integrated observing and assimilation systems for atmosphere, oceans, and land surface, AMS 87th annual meeting. Henry B. Gonzales Convention Center, San Antonio, Texas

Boccaletti G, Pacanowski RC, Philander SG, Fedorov AV (2004) The thermal structure of the upper ocean. J Phys Oceanogr 34:888–902

Brierley C, Fedorov AV, Liu Z, Herbert T, Lawrence K, LaRiviere J (2009) Greatly expanded tropical warm pool and weaker Hadley circulation in the early Pliocene. Science 323:1714–1717

Brown JN, Fedorov AV (2008) Mean energy balance in the tropical Pacific Ocean. J Mar Res 66(1):1–23

Brown JN, Fedorov AV (2010a) How much energy is transferred from the winds to the thermocline on ENSO timescales? J Clim 23:1563–1580

Brown J, Fedorov AV (2010b) Estimating the diapycnal transport contribution to warm water volume variations in the tropical Pacific ocean. J Clim 23:221–237

Collins WD, Bitz CM, Blackmon ML, Bonan GB, Bretherton CS, Carton JA, Chang P, Doney SC, Hack JJ, Henderson TB, Kiehl JT, Large WG, McKenna DS, Santer BD, Smith RD (2006) The community climate system model version 3 (CCSM3). J Clim 19(11):2122–2143

Collins M, S-I An, Cai W, Ganachaud A, Guilyardi E, Jin F-F, Jochum M, Lengaigne M, Power S, Timmermann A, Vecchi G, Wittenberg A (2010) The impact of global warming on the tropical Pacific and El Niño. Nat Geosci 3:391–397

Dawe JT, Thompson L (2006) Effect of ocean surface currents on wind stress, heat flux, and wind power input to the ocean. Geophys Res Lett 33(9)

Delworth TL et al (2006) GFDL's CM2 global coupled climate models. Part I: formulation and simulation characteristics. J Clim 19(5):643–674

Dewitte B, Cibot C, Périgaud C, An S-I, Terray L (2007) Interaction between near-annual and ENSO modes in a CGCM simulation: role of equatorial background mean state. J Clim 20:1035–1052

Fedorov AV (2007) Net energy dissipation rates in the tropical ocean and ENSO dynamics. J Clim 20:1108–1117

Fedorov AV (2010) Ocean response to wind variations, warm water volume, and simple models of ENSO in the low-frequency approximation. J Clim 23:3855–3873

Fedorov AV, Brown JN (2009) Equatorial waves. In: Steele J (ed) Encyclopedia of ocean sciences, 2nd edn. Academic Press, Dublin

Fedorov AV, Philander SG (2000) Is El Niño changing? Science 288:1997–2002

Fedorov AV, Philander SGH (2001) A stability analysis of the tropical ocean-atmosphere interactions: bridging measurements and theory for El Niño. J Clim 14:3086–3101

Fedorov AV, Harper SL, Philander SG, Winter B, Wittenberg AT (2003) How predictable is El Niño? Bull Amer Meteor Soc 84:911–919

Fedorov AV, Pacanowski RC, Philander SGH, Boccaletti G (2004) The effect of salinity on the wind-driven circulation and the thermal structure of the upper ocean. J Phys Oceanogr 34:1949–1966

Fedorov AV, Brierley C, Emanuel K (2010) Tropical cyclones and permanent El Nino in the early Pliocene epoch. Nature 463:1066–1070

Gleckler P, Taylor KE, Dutriaux C (2008) Performance metrics for climate models. J Geophys Res 113:D06104

Goddard L, Philander SG (2000) The energetics of El Nino and La Nina. J Clim 13:1496–1516

Gordon HB, Rotstayn LD, McGregor JL, Dix MR, Kowalczyk EA, O'Farrell SP, Waterman LJ, Hirst AC, Wilson SG, Collier MA, Watterson IG, Elliott TI (2002) The CSIRO Mk3 climate system model [electronic publication]. Aspendale: CSIRO Atmospheric Research (CSIRO Atmospheric Research technical paper; no. 60), pp 130

Griffies SM, Gnanadesikan A, Dixon KW, Dunne JP, Gerdes R, Harrison MJ, Rosati A, Russell J, Samuels B, Spelman MJ, Winton M, Zhang R (2005) Formulation of an ocean model for global climate simulations. Ocean Sci 1:45–79

Gualdi S, Scoccimarro E, Navarra A (2008) Changes in tropical cyclone activity due to global warming: results from a high-resolution coupled general circulation model. J Clim 21:5204–5228

Guilyardi E (2006) El Nino-mean state-seasonal cycle interactions in a multi-model ensemble. Clim Dyn 26:329–348

Guilyardi E, Wittenberg A, Fedorov AV et al (2009a) Understanding El Niño in ocean-atmosphere general circulation models. Bull Amer Meteorol Soc 90:325–340

Guilyardi E, Braconnot P, Li T, Jin F-F, Kim P, Kolasinski M, Musat I (2009b) Mechanisms for ENSO suppression in a coupled GCM with a modified atmospheric convection scheme. J Clim 22:5698–5718

Jin F-F, Kim ST, Bejarano L (2006) A coupled-stability index for ENSO. Geophys Res Lett 33:L23708

Johns TC, Durman CF, Banks HT, Roberts MJ, McLaren AJ, Ridley JK, Senior CA, Williams KD, Jones A, Rickard GJ, Cusack S, Ingram WJ, Crucifix M, Sexton DMH, Joshi MM, Dong B-W, Spencer H, Hill RSR, Gregory JM, Keen AB, Pardaens AK, Lowe JA, Bodas-Salcedo A, Stark S, Searl Y (2006) The new Hadley centre climate model HadGEM1: evaluation of coupled simulations. J Clim 19(7):1327–1353

K-1 model developers (2004) K-1 coupled model (MIROC) description, K-1 technical report, 1. In: Hasumi H, Emori S (eds) Center for climate system research. University of Tokyo, pp 34

Kim ST, Jin F-F (2010) An ENSO stability analysis. Part II: results from the twentieth and twenty-first century simulations of the CMIP3 models. Clim Dyn. doi:10.1007/s00382-010-0872-5

Kim S-J, Flato GM, Boer GJ, McFarlane NA (2002) A coupled climate model simulation of the last glacial maximum, part 1: transient multi-decadal response. Clim Dyn 19:515–537

Large WG, McWilliams JC, Doney SC (1994) Oceanic vertical mixing: a review and model with a nonlocal boundary-layer parameterization. Rev Geophys 32:363–403

Lloyd J, Guilyardi E, Weller H, Slingo J (2009) The role of atmosphere feedbacks during ENSO in the CMIP3 models. Atmos Sci Lett 10:170–176

Marti O, Braconnot P, Bellier J, Benshila R, Bony S, Brockmann P, Cadulle P, Caubel A, Denvil S, Dufresne JL, Fairhead L, Filiberti M-A, Fichefet T, Friedlingstein P, Grandpeix J-Y, Hourdin F, Krinner G, L′evy C, Musat I, Talandier C. IPSL Global Climate Modeling Group 2005. The new IPSL climate system model: IPSL-CM4c

McPhaden MJ (1999) Genesis and evolution of the 1997–98 El Niño. Science 283:950–954

McPhaden MJ, Zebiak SE, Glantz MH (2006) ENSO as an integrating concept in earth science. Science 314:1740–1745

Meehl GA, Gent PR, Arblaster JM, Otto-Bliesner BL, Brady EC, Craig A (2001) Factors that affect the amplitude of El Niño in global coupled climate models. Clim Dyn 17:515

Meehl GA, Covey C, Delworth T, Latif M, McAvaney B, Mitchell JFB, Stouffer RJ, Taylor KE (2007) The WCRP CMIP3 multi-model dataset: a new era in climate change research. Bull Am Meteorol Soc 88:1383–1394

Neale RB, Richter JH, Jochum M (2008) The impact of convection on ENSO: from a delayed oscillator to a series of events. J Clim 21:5904–5924

Oort AH, Ascher SC, Levitus S, Peixoto JH (1989) New estimates of the available potential energy in the world ocean. J Geophys Res 94:3187–3200

Philip S, van Oldenborgh GJ (2006) Shifts in ENSO coupling processes under global warming. Geophys Res Lett 33:L11704

Philip S, van Oldenborgh GJ (2009) Significant atmospheric nonlinearities in the ENSO cycle. J Clim 22:4014–4028

Philip S, van Oldenborgh GJ, Collins M (2009) The role of atmosphere and ocean physical processes in ENSO. Ocean Sci Discuss (submitted)

Roberts WGH, Battisti DS (2010) A new tool for evaluating the physics of coupled atmosphere-ocean variability in nature and in general circulation models. Clim Dyn. doi:10.1007/s00382-010-0762-x

Salas-Mélia D (2002) A global coupled sea ice-ocean model. Ocean Model 4:137–172

Schmidt GA, Ruedy R, Hansen JE, Aleinov I, Bell N, Bauer M, Bauer S, Cairns B, Canuto V, Cheng Y, Del Genio A, Faluvegi G, Friend AD, Hall TM, Hu Y, Kelley M, Kiang NY, Koch D, Lacis AA, Lerner J, Lo KK, Miller RL, Nazarenko L, Oinas V, Perlwitz Ja, Perlwitz Ju, Rind D, Romanou A, Russell GL, Sato M, Shindell DT, Stone PH, Sun S, Tausnev N, Thresher D, Yao M-S (2006) Present day atmospheric simulations using GISS ModelE: comparison to in-situ, satellite and reanalysis data. J Clim 19:153–192

Sun D, Yu Y, Zhang T (2008) Tropical water vapor and cloud feedbacks in climate models: a further assessment using coupled simulations. J Clim 22:1287–1304

Thompson CJ, Battisti DS (2000) A linear stochastic dynamical model of ENSO, part I: development. J Clim 13:2818–2883

Thompson CJ, Battisti DS (2001) A linear stochastic dynamical model of ENSO. Part II: analysis. J Clim 14:445–466

Van Oldenborgh GJ, Philip SY, Collins M (2005) El Niño in a changing climate: a multi-model study. Ocean Sci 1:81–95. Sref:1812-0792/os/2005-1-81

Wang C, Xie SP, Carton JA (2004) Earth's climate. The ocean-atmosphere interaction, vol 147. Geophysical Monograph Series, American Geophysical Union

Wunsch C, Heimbach P (2007) Practical global ocean state estimation. Phys D 230(1–2):197–208

Zhai XM, Greatbatch RJ (2007) Wind work in a model of the northwest Atlantic Ocean. Geophys Res Lett 34(4)